Full Sampling using a Dense Hexagonal Array of Coherent Multi-Beam Detectors

Doug Henke[1*], Stéphane Claude[1], and James Di Francesco[1]
[1]*NRC Herzberg Astronomy and Astrophysics, Victoria, B.C., Canada*
*Contact: Doug.Henke@nrc-cnrc.gc.ca, phone +1-250-363-6937

Abstract— **Using a cold aperture stop, an array of detectors can be arranged to achieve Nyquist spatial sampling. While good aperture efficiency can be obtained, a significant amount of power is truncated at the stop and the surrounding baffling. We analyse the consequence of this power truncation and explore the possibility of using this layout for coherent detection as a multi-beam feed.**

I. Introduction

An important figure of merit for a telescope is mapping speed, i.e., how much time is required to sample fully a given field of view. While single-pixel feeds may be designed to have high aperture efficiencies and excellent receiver sensitivity, in an effort to increase the mapping speed, arrays of detectors may be used to generate more simultaneous beams on sky (i.e., more pixels), at the cost of increased complexity and individual pixel performance degradation [1].

As an introduction, we first define what is meant by the terminology of full sampling with a dense hexagonal array (DHA) of coherent detectors. Coherence implies several things, one of which is that a single-mode detector is used [2]. Accordingly, the telescope is limited to a single spatial mode [3], [4], such that the received signal from a point source is a uniquely defined plane wave at the primary reflector rim and is ideally transformed to the focal plane with resolution limited by the Airy pattern. Of course, a strong motivator for coherent detection is that frequency resolution is preserved. To achieve full sampling, the array follows a hexagonal layout with Nyquist on-sky spacing. Finally, within this paper, a multi-beam array refers to a single optical beam per detector element. In other words, it does not refer to a phased array where one beam is synthesized using several elements.

An important theorem which must hold within our analysis is reciprocity. As applied to an antenna, reciprocity implies that the receive and transmit radiation patterns are reciprocally identical for a given mode and polarisation as long as the antenna system is linear [5]. Reciprocity will be used to analyse the beam coupling to the telescope and also to evaluate the noise added to the receiver.

A. Dense Spacing of Detectors

To sample the field of view fully, Nyquist angular sampling must be achieved. Using a hexagonal layout, the angular on-sky sampling rate is

$$\Delta\theta_{Nyq} = \theta_{FWHM} / \sqrt{3} \approx \lambda / \sqrt{3}\, D \tag{1}$$

where λ is the wavelength and D is the diameter of the primary reflector [6]. When considering the focal plane of the telescope, the feed spacing is then

$$\Delta x_{Nyq} \approx \frac{\lambda}{\sqrt{3}} \frac{f}{D \cdot 1.2} \tag{2}$$

where f is the equivalent focal length of the telescope [6] and the additional factor of 1.2 is an oversampling factor following [7]. Equations (1) and (2) are approximate since the -3 dB beam width, Θ_{FWHM}, is assumed to be λ/D on-sky and $\lambda f/D$ at the focal plane.

The potential problem with packing array feeds at this spacing is twofold: (a) severely reduced aperture efficiency through spill-over losses and (b) possible mutual coupling effects.

Of course, various feeds and trade-offs may be made to pack elements closer, but generally the diameter of the feed horn limits the closest spacing to be on the order of ~ $2\Theta_{FWHM}$ [8] and so the telescope is re-pointed many times (e.g., at minimum 16 times for $2\Theta_{FWHM}$) to fill in extended fields of view due to the sparse sampling. If the feed horn aperture is forced to be smaller to accommodate closer packing density, the resulting beam will simply broaden with respect to the f/D of the telescope and be lost as spill-over power.

Mutual coupling may be overcome by ensuring high isolation between feed ports.

B. Analogies from Incoherent Detectors and the Cold Stop

There are analogies with efficiency and detector spacing for instrumentation design of infrared and optical incoherent detectors. For example, one could consider bolometric detectors and CCDs as suffering from a considerable amount of inherent spill-over, or stray light, but it is mitigated by the use of shrouds, baffles, and stops (see [13] as one example). Therefore, it is interesting to consider whether baffling and stops can be applied to coherent detectors.

We have used the following statement from [1] as motivation for our work:

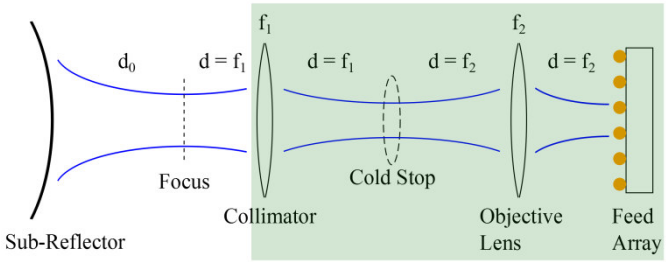

Fig. 1. Simplified unfolded optics demonstrating placement of cold stop. The shaded area represents the portion over which cold, absorbing baffling is used.

Closer spacing is possible if the optical system uses more uniform aperture illumination with the detector beam truncated by a cold Lyot stop. This is a typical method for incoherent THz instruments but has not yet been implemented in a coherent array receiver.

In adopting these concepts for a millimetre-wavelength array, there are several questions. For example, what are the ideal qualities of the baffling and stop? What is the consequence of truncating the power? Where should the stop be placed? Can the receive and transmit paths of the signal be reconciled? What is the effect on the coherency of the signal?

We can philosophically answer each of these questions. Baffling should be implemented so that the spill-over power gets absorbed without reflection to keep feeds isolated. Reciprocally, the termination can be thought of as noise power emitted into the receiver, so it is important that its physical temperature is some fraction of the equivalent receiver noise temperature. By making use of a collimator within the array, a stop may be placed at the point at which all beams coincide, i.e., the *optical waist*, such that each beam is truncated equally [14]. The stop needs to be evaluated (also using reciprocity) to analyse the characteristics of the diffracted beam through the stop and to calculate the resulting single mode aperture efficiency to validate the coherency of the detector. It is also useful to separate the spill-over power along the optical path into two contributions: (1) the spill-over power commonly associated with aperture efficiency which is evaluated at the primary reflector of the telescope and (2) the power intercepted by the cold absorbing baffles and aperture stop.

II. Analysis

A. Simplified Quasioptical Design

It is useful to consider the example frequency of ALMA Band 3 (84–116 GHz) to explore the impacts of a cold stop within a dense multi-beam array. A simplified example is shown in Fig. 1 where a collimator has been used after the telescope focus and then reimaged onto the detector array.

Baffling is indicated within the figure, shown by the shaded area, and represents the region over which any scattered power is terminated by absorber at cryogenic temperature. The beam outside of the shaded area is treated separately as aperture efficiency of the telescope (including its own spill-over efficiency term).

TABLE 1
BEAM PARAMETERS AS DETERMINED BY FUNDAMENTAL MODE QUASIOPTICS

Frequency (GHz)	Sub-Reflector	Cassegrain Focus	Collimator Lens	Stop	Object Lens	Detector Array
Distances with respect to Focus (mm)						
84	-6000.0	0.0	157.8	315.6	473.4	631.2
100	-6000.0	0.0	157.8	315.6	473.4	631.2
116	-6000.0	0.0	157.8	315.6	473.4	631.2
Beam Radii (mm)						
84	319.0	21.4	23.5	8.41	22.4	21.4
100	319.0	17.9	20.2	8.40	19.4	17.9
116	319.0	15.5	18.0	8.40	17.2	15.5
Radii of Curvature (mm)						
84	-6000.0	6000.0	1051.4	-929.7	178.6	6000.0
100	-6000.0	6000.0	817.2	-1315.8	189.1	6000.0
116	-6000.0	6000.0	662.1	-1769.1	201.3	6000.0

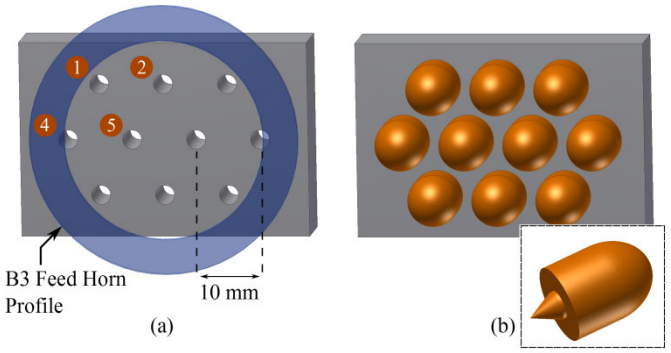

Fig. 2. Examples of simple detector feeds for a dense array: (a) circular waveguides, and, (b) circular waveguides with extended elliptical lenses (inset). Each feed is arranged in a hexagonal layout and the circular waveguides are modelled within a simple metallic box. Simulation port numbers are indicated in (a) and represented by encircled numbers. Because of symmetry, it is sufficient to consider only ports 1, 2, 4, and 5. For comparison, the ALMA Band 3 receiver feed horn inner and outer profiles are shown to emphasize the compactness of the array element spacing.

Using quasioptics [12], the ideal beam characteristics may be found by working backwards from the sub-reflector assuming that the edge taper and focus are constant over frequency when evaluated at the sub-reflector. Given the layout described in Fig. 1, the design is summarized in Table 1. In this design, the distance between the focal plane and sub-reflector is assumed to be 6 m and distances are given with respect to the focal plane in the direction towards the detector array. Also note that no truncation has been modelled within Table 1.

B. Feed Spacing and the Detector Array

Next, it is important to consider what type of feed can be realized. To sample the field of view fully at the highest frequency of 116 GHz, from (2) the spacing should be set at ~10 mm. Clearly there is no possibility to use an array of feed horns to achieve this compact spacing. For example, the current ALMA Band 3 receiver feed horn, shown for reference in Fig. 2, has an inner diameter of approximately 30 mm [15]!

Ideally, the array feeds should be simple, support dual linear polarization, and exhibit excellent port-to-port isolation. To demonstrate the importance of the feeds, two examples will be used for the dense hexagonal arrays (DHA). A simple array of circular waveguides, as shown in Fig. 2(a), could be used since they show good input reflection and isolation. To reduce the amount of power that is terminated with baffles and

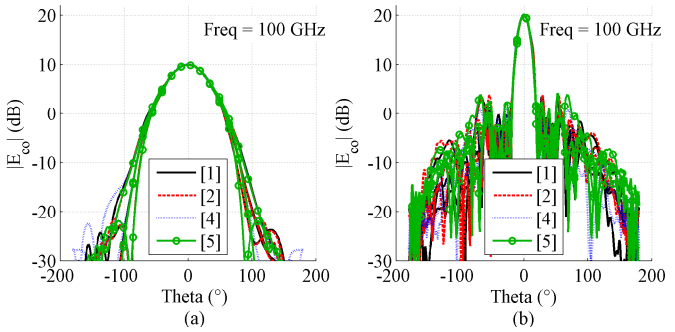

Fig. 3. Comparison of co-polar far-fields for the respective dense hexagonal array (DHA) models shown in Fig. 2 (a) and (b), simulated at 100 GHz. Each plot contains the respective fields for ports 1, 2, 4, and 5 (labelled in brackets) and show field cuts overlapping at angles of phi = 0, 45, 90, and 135°.

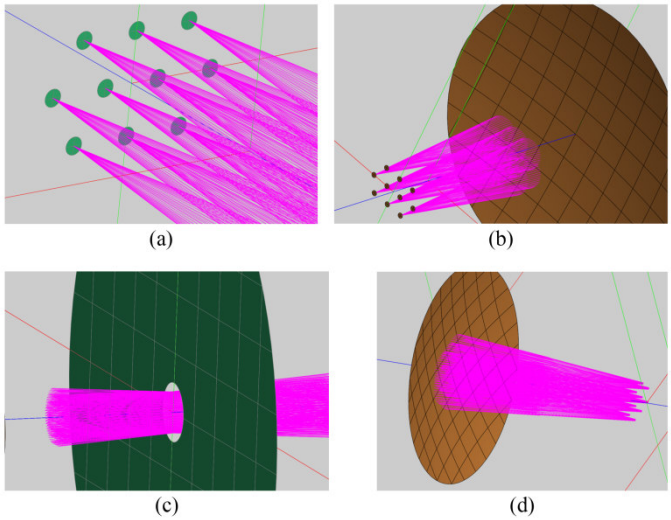

Fig. 4. Simplified GRASP implementation for the DHA models shown in Fig. 2. Each detector output has been represented by simple ray optics, using narrow beams for clarity. The layout follows the structure shown in Fig. 1 except the lenses are represented by reflectors and the beam is folded back. For clarity, the beams of the folded optics have been divided up to show: (a) the hexagonal layout of the detector feeds, (b) the off-axis beams illuminating the objective mirror, (c) the beams converging to share a common "optical waist" (coincident with the placement of the aperture stop), and (d) the output beams of the collimator to illustrate reimaging onto the focal plane.

absorber, however, it is advantageous to try to increase the directivity of the beams. One simple method is to use an extended elliptical lens at the aperture [16] as shown in Fig. 2(b). The simulated S-parameters of each model show port reflection is less than -20 dB and port-to-port isolation is less than -30 dB.

Fig. 3 demonstrates the difference in the far-fields of the feed arrays themselves when the extended elliptical lenses are used. In comparison to open-ended circular waveguides, the beams are narrower, more symmetric, and exhibit ~10 dB more gain. The added penalty, however, is an increased side-lobe value. For comparison, a single-pixel feed designed for the ALMA 12-m telescopes would have an opening half-angle of 3.58°. As such, both of the feeds shown in Fig. 3 are extremely broad and require careful attention to the spill-over power at each element along the optical path.

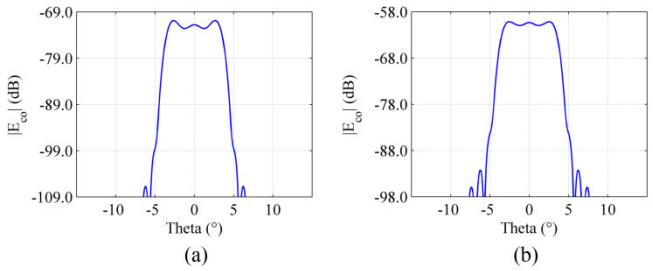

Fig. 5. Co-polar near-field radiation patterns evaluated at the sub-reflector rim for open-ended circular waveguides (a) and extended elliptical lenses (b).

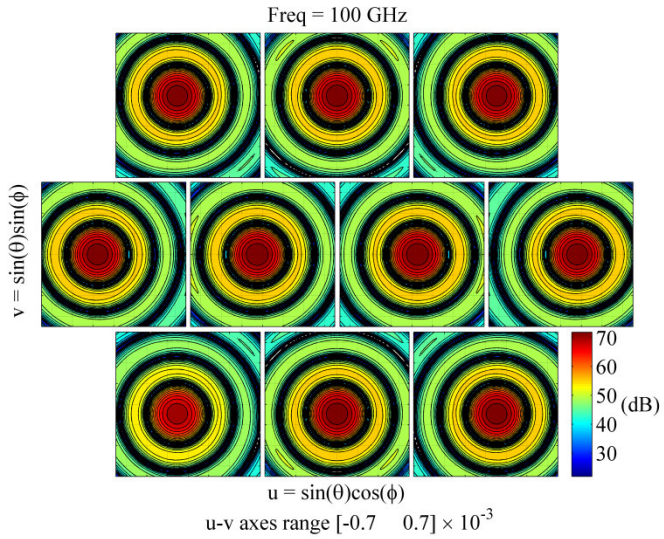

Fig. 6. Co-polar far-field projections on-sky of each feed port for the extended elliptical lens model through the optical system (stop radius = 11 mm). Each beam is plotted separately, but shown in their respective position according to Fig. 2.

C. Simplified GRASP Implementation

1) Optical Path and Detector Layout

As a first step towards verification, the dense hexagonal array (DHA) models of Fig. 2 were simulated using GRASP. In this preliminary approach, all reflecting optics are on-axis and the unfolded optics described in Fig. 1 are folded back along the axis (shadowing is not included in this simplified analysis). Fig. 4 describes the approach used. Although not shown, an equivalent paraboloid is used to represent an ALMA telescope with a focal length of 96 m and diameter of 12 m.

2) Transmit Radiation Patterns Along the Optical Path

Continuing with the transmit path of the telescope (i.e., the detector array transmitting), the output beam was evaluated at the sub-reflector and is plotted in Fig. 5 for the two types of feeds being considered.

In this analysis, the aperture stop radius has been set to 11 mm (found to optimise the aperture efficiency) and is plotted with respect to a normalised feed power of 4π. Note that the output of the collimator evaluated at the sub-reflector, as shown in Fig. 5, results in a radiation pattern that

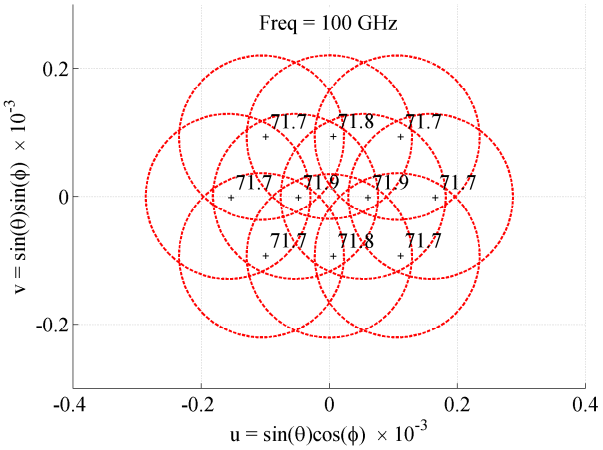

Fig. 7. -3 dB contours of the simulated co-polar far-field, as shown in Fig. 6 and evaluated at 100 GHz, but plotted within the same axes. Peak values, given in dB and normalised with respect to each feed array element, are given for each beam.

TABLE 2
CALCULATED APERTURE EFFICIENCY FOR THE DHA MODELS OF FIG. 2 (A) AND (B) USING THE 4TH FEED PORT AND AN OPENING ANGLE OF 3.58°.

Frequency (GHz)	Feed Element	η_{spill}	η_{amp}	η_{cross}	η_{phase}	η_{total}
84	4 (a)	0.893	0.983	1.000	0.989	0.868
100		0.875	0.992	1.000	0.987	0.857
116		0.884	0.992	1.000	0.990	0.868
84	4 (b)	0.893	0.986	1.000	0.993	0.874
100		0.890	0.992	1.000	0.991	0.875
116		0.894	0.992	1.000	0.991	0.879

approaches a top-hat response, suggesting that the beam provides high aperture efficiency.

Next, we consider the resulting far-fields of the telescope for the entire DHA. Fig. 6 shows the simulated co-polar far-field for each feed within the detector array when the extended elliptical lenses are used. Each subplot within the figure corresponds to the position of a feed element within the array. In Fig. 7, all simulated feed patterns have been plotted within the same u-v axes, but only showing the -3 dB contours for clarity. The HPBW contour circles correspond nicely with the expected spacing and show dense spatial sampling; since the spacing is set for the highest frequency, full sampling is observed at 116 GHz and oversampling at lower frequencies. Symmetry is evident and the resulting beams are encouraging since all beams are similar, indicating that the aperture stop is located properly and affecting each feed element somewhat equally. For brevity, Fig. 6 and Fig. 7 only show the results of the elliptical lens model, but similar results are found for the open waveguides except with lower gains.

3) Aperture Efficiency at the Output of the Collimator

Next, it is useful to look at the resulting aperture efficiency of the output beam of the aperture stop. The aperture efficiency is calculated using an overlap integral [9], [17] and is calculated at the rim of the sub-reflector with respect to the focal plane of the telescope. Note that the scattered or intercepted power between the feed array and collimator is not included within this calculation. Only the field at the sub-reflector rim is used and normalised accordingly. Given the simplifications of the model shown within this section, no back-scattering is included and the signal is assumed to be fully contained within Θ ranging from 0–90°. Again, a stop aperture radius of 11 mm has been used. As shown in Table 2, the resulting aperture efficiency of the formed beam is very good (with the important caveat that the truncated power between the collimator and the feed has not yet been accounted for).

TABLE 3
CUMULATIVE POWER ALONG THE OPTICAL PATH FOR THE MODELS OF FIG. 2 (A) AND (B), USING THE 4TH FEED ELEMENT AND CALCULATED FOR 100 GHZ.

Feed Element	Objective Mirror	Stop	Collimator	Equivalent Paraboloid
4 (a)	43.23%	41.91%	1.14%	1.02%
4 (b)	77.07%	65.89%	10.53%	9.56%

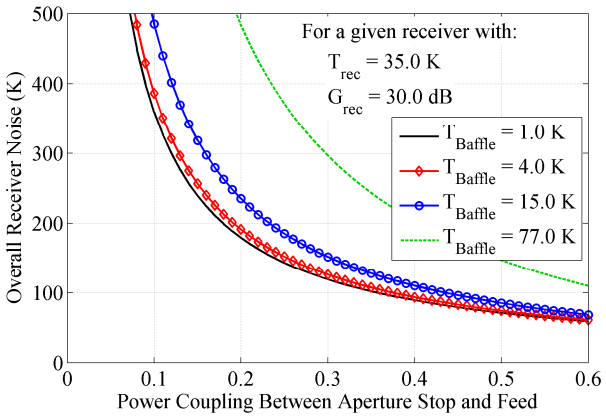

Fig. 8. Effect of coupling loss when the baffling structures, which terminate the lost power, are held at different physical temperatures.

4) Cumulative Power Along the Transmit Path

Since we are using dense feeds with very broad radiation patterns, one main point of interest is how to treat the power that is truncated by the baffling and aperture stop. Using GRASP, the array feed element may be excited to calculate the amount of intercepted power within the shaded region of Fig. 1. The intercepted power is also, by reciprocity, the amount of power coupled into the detector with respect to the beam received at the collimator.

Table 3 shows the amount of power intercepted by each object along the optical path, as described in Fig. 1 and Fig. 4, when the radius of the aperture stop is 11 mm. Considering first the open-ended waveguides, (a), only ~43% of the power is intercepted by the objective lens. Then, most of the remaining power is absorbed at the cold stop so that only ~1% of the overall power actually arrives at the collimator mirror. Looking next at the elliptical lenses, (b), significantly more power is retained through the system, yet still only ~10% arrives.

Herein lies the major hurdle towards acceptable performance for radio astronomy which the two feed models aptly illustrate. Since the assumption is made that the baffling and absorbing aperture stop are held at cryogenic temperatures, the optical coupling loss (i.e., the cumulative power received at the collimator shown in Table 3) may be

TABLE 4
COMPARISON OF SYSTEM NOISE BETWEEN A SINGLE-PIXEL RECEIVER AND AN ELEMENT WITHIN A FULLY SAMPLED DHA WITH ELLIPTICAL LENSES.

Frequency (GHz)	τ_0	T_{sky}	Single Pixel		$\frac{Nyquist}{1.2}$ DHA		$(T_{sys}$ Ratio$)^2 \leftrightarrow \tau_{int}$
			T_{rec}	T_{sys}	T_{rec}	T_{sys}	
84	0.048	12.924	35	67.1	483	561.9	70.1
100	0.054	14.196	35	68.9	368	438.8	40.6
116	0.336	69.531	35	168.7	275	522.3	9.6

effectively considered as a cold attenuator at the input of a receiver chain. Fig. 8 illustrates the consequence to overall receiver noise when the scattered power (i.e., power that is lost due to coupling losses) is terminated by the baffling at various physical temperatures. For illustration, it is assumed that the receiver element has an equivalent noise temperature of 35 K, representative of the ALMA B3 receiver cartridge [18]. By separating out the contribution of the power lost due to the baffling, the importance of the feed directivity is highlighted. One can see that although both feed models provide good feed isolation and aperture efficiency after the aperture stop, the coupling loss—even if the baffling is held at cryogenic temperatures—significantly degrades the resulting overall receiver temperature. In fact, the open-ended waveguides result in an overall receiver noise that is off the chart in Fig. 8 and the extended elliptical lens array shows a factor of ~10 degradation.

To relate this degradation in terms of integration time, the system temperature must be known. From [7], neglecting background terms and pointing at zenith, the system temperature is

$$T_{sys} = \frac{1}{\eta_{eff} e^{-\tau_0}} \left(T_{rec} + \eta_{eff} T_{sky} + \left(1 - \eta_{eff}\right) T_{amb} \right) \quad (3)$$

where η_{eff} is the forward efficiency (fixed at 0.95 in [7]), $e^{-\tau o}$ is the fractional transmission of the atmosphere, T_{sky} is the sky temperature, and T_{amb} is the ambient temperature (fixed at 270 K in [7]).

Using the ALMA Sensitivity Calculator (ASC)[1], values of sky temperature and atmospheric transmission can be found and are shown in Table 4. Typical observing conditions are used for ALMA Band 3, i.e., a water vapour column density of 5.1 mm is assumed.

Also in Table 4, the last column shows the comparative increase in integration time between a single-pixel receiver and a DHA element (since integration time is proportional to the square of system noise temperature). Note that within the ALMA Band 3 frequency range, the upper frequency has considerably more atmospheric attenuation due to the water and oxygen absorption lines nearby. Since the sky noise temperature dominates the receiver noise temperature at the highest frequency, variations in receiver noise have less impact on overall system integration time.

Depending on how dominant the sky noise is, ~10–70 fully sampled DHA elements are required just to have equivalent single-pixel performance (notwithstanding raster scanning time for single-pixel extended fields of view). Note that with less compact spacing, the feed element aperture area may be increased so that the design may be shifted along the power coupling axis of Fig. 8 to trade-off spacing with overall receiver noise.

[1] https://almascience.nrao.edu/proposing/sensitivity-calculator

III. CONCLUSIONS AND FUTURE WORK

An optical layout has been presented to explore the ramifications of full spatial sampling with multi-beam feeds using compact hexagonal spacing. Two different feed array models have been shown that exhibit the desired characteristics of simplicity, dual-linear polarization, good port match, high feed isolation, good aperture efficiency, and full Nyquist spatial sampling. The two models differ, however, in the amount of power lost in the cold baffling and absorbing aperture stop. By separately treating the scattered power between the aperture stop and feed array, the importance of feed directivity is highlighted through representing the coupling loss as cold attenuation at the receiver input. Since directivity is fundamentally limited by the feed aperture area, extremely compact array spacings will suffer as shown above.

It should be noted that the spacing presented within this paper is extremely compact for coherent detectors, as the spacing was set for the highest frequency within the band—even with an oversampling factor at the highest frequency. Using a cold aperture stop would also allow the designer to pick a wider spacing which is still much more compact than existing heterodyne arrays, e.g., a spacing of $2\Delta x_{Nyq}$ would imply only 4 separate telescope pointings to completely fill in the array field of view. Wider spacing would enable larger feed apertures (or larger lens diameters) to improve directivity of the beams and, therefore, shift the power coupling and drop the overall receiver noise, according to Fig. 8.

Future work will examine the system performance for less compact spacings, e.g. $2\Delta x_{Nyq}$, and will also explore possible improvements by changing the type of aperture stop and optimizing the directivity of the feed elements.

ACKNOWLEDGMENT

The authors would like to acknowledge: J. Atwood and J. Pazder for interesting conversations about optics fundamentals and T. Hardy and J.-P. Veran for informative discussions of optical detectors.

This material is based upon work supported by Associated Universities, Inc./National Radio Astronomy Observatory and the National Science Foundation under Cooperative Agreement No. AST-0836064.

REFERENCES

[1] C. E. Groppi and J. H. Kawamura, "Coherent Detector Arrays for Terahertz Astrophysics Applications," *IEEE Trans. THz Sci. Technol.*, vol.1, no.1, pp. 85–96, Sept. 2011.

[2] J. Lesurf, *Millimetre-wave Optics, Devices and Systems*, England: IOP Publishing Ltd., 1990.

[3] J. Murphy and R. Padman, "Focal-Plane and Aperture-Plane Heterodyne Array Receivers for Millimeter-Wave Radioastromony—A Comparison," *Int. J. Infrared Millim. Waves*, vol. 9, no. 8, Aug. 1988.

[4] P. F. Goldsmith, C.-T Hsieh, G. R. Huguenin, J. Kapitzky, and E. L. Moore, "Focal plane imaging systems for millimeter wavelengths," *IEEE Trans. Microw. Theory Techn.*, vol. 41, no. 10, pp. 1664–1675, Oct. 1993.

[5] C. A. Balanis, *Antenna Theory: Analysis and Design*, 2nd ed., New York: John Wiley & Sons, Inc., 1997.

[6] J. F. Johansson, “Fundamental limits for focal-plane array efficiency,” in *Proc. Multi-Feed Systems for Radio Telescopes, ASP Conf.*, vol. 75, pp. 34–41, 1995.

[7] A. Lundgren, “ALMA Cycle 2 Technical Handbook”, ver. 1.1, 2013. http://www.almascience.org.

[8] P. F. Goldsmith, "Focal plane arrays for millimeter-wavelength astronomy," in *IEEE MTT-S Int. Microw. Symp. Dig.*, vol. 3, pp.1255–1258, Jun. 1992.

[9] J. W. Lamb, "Low-noise, high-efficiency optics design for ALMA receivers," *IEEE Trans. Antennas Propag.*, vol. 51, no. 8, pp. 2035–2047, Aug. 2003.

[10] R. Padman, “Optical fundamentals for array feeds,” in *Proc. Multi-Feed Systems for Radio Telescopes, ASP Conf.*, vol. 75, pp. 3–26, 1995.

[11] R. Padman, J. A. Murphy, and R. E. Hills, “Gaussian mode analysis of Cassegrain antenna efficiency,” *IEEE Trans. Antennas Propagat.*, vol. AP-35, pp. 1093–1103, Oct. 1987.

[12] P. F. Goldsmith, Quasioptical Systems: Gaussian Beam Quasioptical Propagation and Applications. New York: IEEE Press, 1998.

[13] J. Glenn, P. Ade, M. Amarie, J. Bock, S. Edgington, A. Goldin, S. Golwala, D. Haig, A. Lange, G. Laurent, P. Mauskopf, M. Yun, and H. Nguyen, “Current status of Bolocam: a large-format millimeter-wave bolometer camera,” in *Proc. SPIE 4855, Millim. Submillim. Detectors Astron.*, vol. 4855, no. 30, Feb. 2003.

[14] B. Weiner. (2008, Sept.). Scaling relations for telescopes, spectrographs, and reimaging instruments. Stewart Observatory, University of Arizona. Tuscon, Arizona. [Online]. Available: http://mingus.as.arizona.edu/~bjw/spectrographs/spectrographs.pdf

[15] M. Carter, et al., “ALMA front-end optics design report,” Nat. Radio Astron. Observatory, Charlottesville, VA, ALMA EDM Doc. FEND-40.02.00.00-035-B-REP, Jul. 2007.

[16] D. F. Filipovic, S. S. Gearhart, G. M. Rebeiz, “Double-slot antennas on extended hemispherical and elliptical silicon dielectric lenses," *IEEE Trans. Microw. Theory Techn.*, vol. 41, no. 10, pp. 1738–1749, Oct. 1993.

[17] K. Pontoppidan, “Electromagnetic properties and optical analysis of the ALMA antennas and front ends,” Nat. Radio Astron. Observatory, Charlottesville, VA, ALMA EDM Doc. FEND-80.04.00.00-026-A-REP, Jan. 2008.

[18] S. Claude, P. Niranjanan, F. Jiang, D. Duncan, D. Garcia, M. Halman, H. Ma, I. Wevers, and K. Yeung, “Performance of the production band 3 receivers (84–116 GHz) for the Atacama Large Millimeter Array (ALMA), *Int. J. Infrared Millim. Waves*, vol. 35, no. 6-7, pp. 563–582, Jul. 2014.